Original article

Synthesis and biocompatible role of hierarchical structured carbon nanoplates incorporated α-Fe₂O₃ nanocomposites for biomedical applications with respect to cancer treatment

Mohamad S. AlSalhi [a,*], Sandhanasamy Devanesan [a], Paramasivam Shanmugam [b], Young Ock Kim [c], Jun-Tac Kwon [d], Hak-Jae Kim [d,*]

[a] Department of Physics and Astronomy, College of Science, King Saud University, P.O. Box -2455, Riyadh 11451, Saudi Arabia
[b] Department of Chemistry, St. Joseph University, Dimapur 797115, Nagaland, India
[c] Department of Bio-Environmental Chemistry, College of Agriculture and Life Sciences, Chungnam National University, 99 Daehak-Ro, Yuseung-Gu, Daejeon 34134, Republic of Korea
[d] Department of Clinical Pharmacology, College of Medicine, Soonchunhyang University, Cheonan, Republic of Korea

ARTICLE INFO

ABSTRACT

This study aimed to inspect the hierarchically structured spherical-like hematite (α-Fe₂O₃) nanoparticles synthesize by simple, low temperature solution combustion process. The uniformly distributed α-Fe₂O₃/carbon nanocomposite (α-Fe₂O₃/C nanocomposite) was prepared by incorporating carbon nanoplates into sphere-like α-Fe₂O₃ nanoparticles. The synthesized nanomaterials were characterized using various techniques such as XRD, FESEM, and EDS. The cytotoxicity of the material was evaluated by MTT assay and nuclear imaging based on the cell morphological changes on both human lung cancerous cell line A549 and chang liver as non cancerous cell line. The results demonstrated that the pure and composite material exhibited above 70% viability on non-cancerous cell line and around 60% inhibition on A549 lung cancer cell line indicates the α-Fe₂O₃/C nanocomposite is biocompatible and can be used for biological applications and anticancer therapy. Cell death induced by α-Fe₂O₃, carbon nanoplates and α-Fe₂O₃/C nanocomposites was further evidenced with DAPI.

© 2019 The Author(s). Published by Elsevier B.V. on behalf of King Saud University. This is an open access article under the CC BY-NC-ND license (http://creativecommons.org/licenses/by-nc-nd/4.0/).

1. Introduction

In recent decade, nanoscience and nanotechnology has created scope to manufacture, and uncommonly modify the efficient properties of nanomaterials for biological applications. The nanomaterials are the intermediates among the solid states and atomic/molecular, which combine chemical availability in arrangement with physical assets of the bulk phase Wilkinson, 2003. The essential progress of nanomaterials and its nanocomposites have discovered their utilization in a broad assortment of fields such as data storage, energy conversion, electro/photocatalysis, MRI, gas sensors, bioseparation, wastewater treatment, biomedicine and so on [Bhattacharya et al., 2014; Andiappan et al., 2019; Andiappan et al., 2018; Wei et al., 2018; Sanmugam et al., 2017]. Among the various transition metal oxides, the iron oxide nanomaterials with unique magnetic properties have been practised well in biomedical applications. More recently, an enlarged research with different types of iron oxides have been investigated in the wide research of magnetic particles [Theerthagiri et al., 2013; Patsula et al., 2016; Basith et al., 2016; AlSalhi et al., 2016]. In view of biocompatibility applications, γ-Fe₂O₃ and Fe₃O₄ are very promising candidates because they are well thought-out to be kind in the human body as they eagerly dissociate under the condition of acidic nature.

Very limited work carried out using α-Fe₂O₃ for biocompatibility studies. For example, Rajendran et al. (2017) synthesized α-Fe₂O₃ nanoparticles via biosynthesis process and utilized for the cytotoxicity studies against Hep3B, A549, MCF-7 and Vero cell lines. They found that α-Fe₂O₃ nanoparticles were good biocompatible as they didn't cause hemolysis of RBC. Cardillo et al. (2016) synthesized α-Fe₂O₃ by two different synthetic conditions to get different surface morphology. They have investigated and

reported the surface morphology of the nanoparticles against the biocompatibility studies using Madin-Darby Canine Kidney cell line. Kanagesan et al. (2013), synthesized α-Fe$_2$O$_3$ nanoparticles by low temperature combustion process and studied for the cytotoxicity of the material against human breast cancer MCF-7 cell line. They reported that α-Fe$_2$O$_3$ nanomaterials exhibit no toxic effect. Another report by Rajendran et al. (2015) prepared α-Fe$_2$O$_3$ nanoparticles by biosynthesis process and evaluated for its cytotoxic effect against HepG2 liver cells by MTT assay. They reported that the α-Fe$_2$O$_3$ nanoparticles with size of 30 nm, displayed a considerable cytotoxicity activity for HepG2 cells.

In the present study, hierarchically structured spherical-like α-Fe$_2$O$_3$ were prepared by simple, low temperature solution combustion route and carbon nanoplates incorporated α-Fe$_2$O$_3$ (α-Fe$_2$O$_3$/C) nanocomposite was prepared via a low-cost wet chemical process. In this investigation, carbon nanoplates were chosen to incorporate α-Fe$_2$O$_3$ because it's a distinctive element with excellent assets such as flexibility, low-cost, resistance to acidic and basic conditions, low density, electrical conductivity, and tensile. As per our knowledge, there is no work on the cytotoxicity activity of α-Fe$_2$O$_3$/C nanocomposite against A549 cells and Chang liver cell lines. The cytotoxicity activity of the synthesized nanomaterials was evaluated against A549 cells and Chang liver cell lines using MTT assay. The surface structure of the nanomaterials such as nanoplates and spherical particles exhibited minimal cytotoxicity activity.

2. Materials and methods

2.1. Reagents

Fe(NO$_3$)$_3$·9H$_2$O was purchased from Qualigens India. Carbon nanoplate powder was obtained from Cabot Corporation, USA. DAPI and trypsin were purchased from Sigma-Aldrich, USA. DMSO, dulbecco's modified eagle's medium (DMEM), fetal bovine serum (FBS), MTT, DAPI, Propidium Iodide (PI), trypan blue, phosphate buffer saline (PBS) and citric acid (C$_6$H$_8$O$_7$) were obtained from Himedia, India. All chemical reagents were used without further purification.

2.2. Synthesis of spherical-like α-Fe$_2$O$_3$ nanoparticles

Hierarchically structured spherical-like α-Fe$_2$O$_3$ were prepared by a solution combustion process using Fe(NO$_3$)$_3$·9H$_2$O as a iron source and C$_6$H$_8$O$_7$ as the fuel. The synthesis procedure for the spherical-like α-Fe$_2$O$_3$ nanoparticles was adopted and modified our previous report [20]. For instance, calculated stoichiometric amount of Fe(NO$_3$)$_3$·9H$_2$O (1 mol) and C$_6$H$_8$O$_7$ (3 mol) were dissolved in 100 mL of distilled water. The reaction mixture was homogeneously mixed well and subsequently evaporated the solvent at 85 °C. Then, the acquired iron-citrate precursor powder was ignited at 500 °C for 2 h to get spherical-like α-Fe$_2$O$_3$ nanoparticles. The schematic illustration for the synthesis of spherical-like α-Fe$_2$O$_3$ nanoparticles is exhibited in Fig. 1.

2.3. Synthesis of α-Fe$_2$O$_3$/C nanocomposites

α-Fe$_2$O$_3$/C nanocomposites was prepared by simple wet chemical route. In a typical preparation, calculated 3 weight percentages of carbon nanoplates with respect to α-Fe$_2$O$_3$ and as-synthesized α-Fe$_2$O$_3$ nanoparticles was mixed well into 20 mL of ethanol in a beaker. Then, the beaker was placed in an ultrasonic bath for 20 min. Finally, the obtained reaction mixture was magnetically stirred well and consequently the absolute ethanol was allowed to evaporate at 60 °C. The obtained α-Fe$_2$O$_3$/C nanocomposite after volatilization of the absolute ethanol was dried at 100 °C for 5 h.

2.4. Insrumental charctaerizations

The structure and formation of the samples was obtained by power XRD method using a Rigaku/Mini Flex II diffractometer with CuKα (λ = 0.1542 nm) radiation. The FT-IR spectra was examined using a JASCO 460 plus model instrument. The structural morphology of the synthesized samples was analyzed using FESEM (Hitachi, S-4800) at 20 kV. The elemental composition analysis was observed using EDS-Bruker Nano GmbH, X Flash Detector, model 5010 instrument equipped with FE-SEM.

2.5. Cell culture

Human lung carcinoma cell line A549 and non cancerous cell line (chang liver) was procured from NCCS, Pune for this study. The cell lines was cultured in 10% Dulbecco's modified Eagle's medium added with (DMEM) 50 IU/mL penicillin and 50 mg/mL streptomycin. The cultures were maintained at 37 °C, with 5% CO$_2$ in 25 cm^2 flasks. The cells were sub cultured by 0.25% trypsin, 1 mM EDTA and resuspended in fresh medium. Cells were counted using trypan blue dye exclusion process in a hemocytometer and seeded in new plates.

2.6. Cytotoxicity assay

The cellular toxicity of α-Fe$_2$O$_3$, carbon nanoplates and α-Fe$_2$O$_3$/C nanocomposites were studied using MTT assay in two different cell lines. The samples were dispersed in sterile DMEM medium to get a concentration of 1 mg/mL. The medium without sample served as blank. The cells were trypsinized and seeded in 96 well plate at a density of 1.2×10^3 cells. After 24 h incubation the cells were suspended with fresh medium and treated with α-Fe$_2$O$_3$, carbon and α-Fe$_2$O$_3$/C nanocomposite at different concentration range from 10 to 50 μg/mL. After 48 h treatment the samples were removed and 20 μL of MTT (5 mg/mL) was added and incubated for 3.5 h. Thereafter, MTT was carefully removed and the purple crystals was dissolved using 150 μL of DMSO. The samples were agitated for 15 min and the absorbance was read at 570 nm using multiplate reader. The relative cell viability (%) was estimated by the following equation.

$$\% \; Cell \; viability = \frac{\text{A(Test sample)}}{\text{A(control)}} \times 100 \qquad (1)$$

Where, A is absorbance. The experiment was carried out in triplicates and the results was expressed as mean deviation ± standard.

2.7. Morphological changes

Cancerous cell line A549 and noncancerous cells (Chang liver) was seeded in 24 well plate and then administrated with α-Fe$_2$O$_3$, carbon nanoplates and α-Fe$_2$O$_3$/C nanocomposites for 24 h. After the 24 h adminstration the cells were captured with an inverted flurecence microscope (EVOS fl) stained with Propodium Iodide (PI) for chang liver cells and DAPI staining for A549 Cells. Changes in the cell nuclear morphology were indicated the cytotoxic effect of the nano meterial on both the cell lines.

The cells were stained using DNA binding dye PI. The nanoparticles treated cells was washed with PBS and incubated with PI stain for 2–3 min. After, the samples were rinsed with PBS twice and observed under fluorescence microscope; Similarly, DAPI staining was done on nanoparticles treated cells. After incubation with nanomaterials, cells were stained with DAPI for 2 min, then
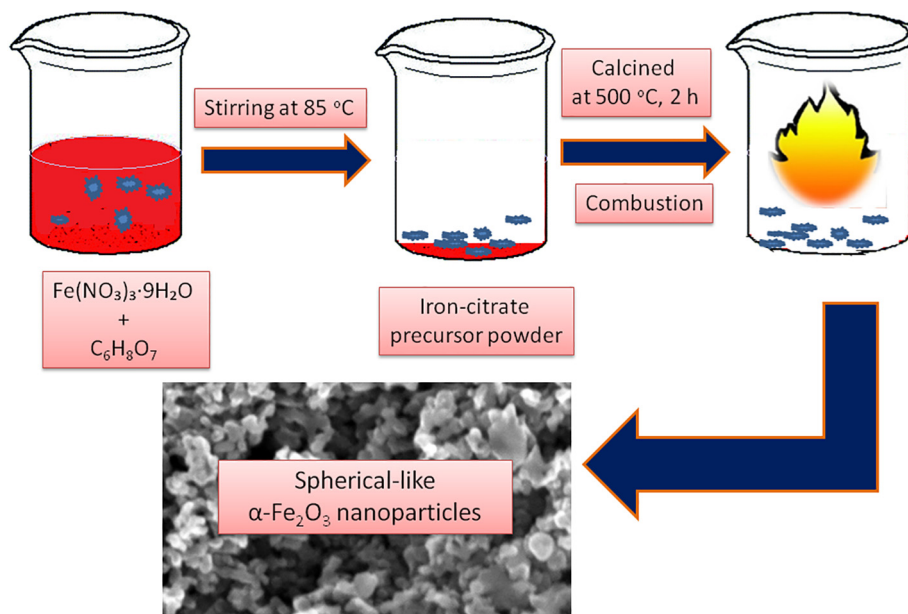
Fig. 1. The schematic demonstration of spherical-like α-Fe₂O₃ nanoparticles synthesis using solution combustion process.

rinsed with PBS and cells were visualized and captured by inverted flurecence microscope (EVOS fl).

3. Results and discussion

3.1. XRD studies

The phase structure and formation of the synthesized samples was analysed using powder XRD and the corresponding XRD patterns of α-Fe₂O₃, carbon nanoplates and α-Fe₂O₃/C nanocomposites are displayed in Fig. 2. The observed diffraction of α-Fe₂O₃ (Fig. 2a) exhibited at 2θ = 24.07°, 33.17°, 35.39°, 40.81°, 49.20°, 54.37°, 57.32°, 62.50°, and 63.97°, are in well correlated to the resultant diffraction of rhombohedral phase of α-Fe₂O₃ (JCPDS
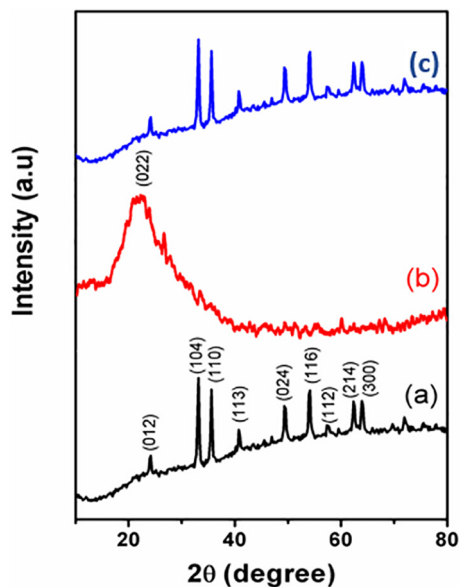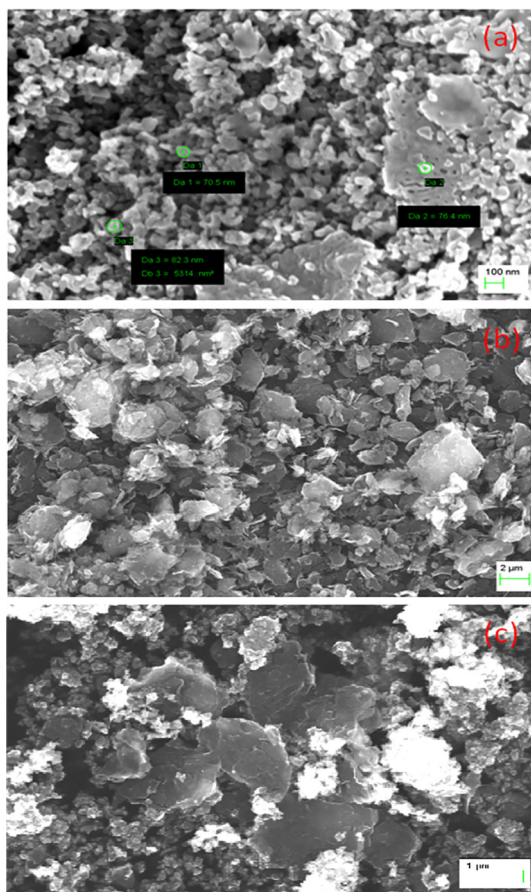
No. 80-2377) which was also fine agreement with our earlier reports [Theerthagiri et al., 2014; Senthil et al., 2018]. The diffraction pattern for pure carbon nanoplates (Fig. 2b) shows distinct broad peaks at 2θ = 22.60°. The broad diffraction peak indexed as (0 2 2) which indicate the existence of amorphous nature of the carbon particles Rajan et al., 2014. The diffraction patterns of α-Fe₂O₃/C nanocomposites is depicted in Fig. 2(c), which exposed that the XRD of pure α-Fe₂O₃ was unchanged due to the addition of carbon nanoplates. In addition, it exhibits that the intensity of diffraction peaks was slightly reduced however it was interesting to observe that the carbon peak didn't appear which might be because of the way that it was available in low detection level of XRD technique and furthermore low amount of carbon added into α-Fe₂O₃ in the nanocomposite sample [Theerthagiri et al., 2016]. The crystalline size of the synthesized materials was calculated using Scherrer's equation. The observed crystallite size of the pure α-Fe₂O₃, carbon nanoplates and α-Fe₂O₃/C nanocomposites was found to be around 26.50, 5.12, and 30.24 nm, respectively.

3.2. Morphology structure and elemental studies

The structural morphology of the synthesized α-Fe₂O₃, carbon nanoplates and α-Fe₂O₃/C nanocomposites was analyzed using FESEM and the consequential picture are displayed in Fig. 3. The pristine α-Fe₂O₃ sample (Fig. 3a) showed the spherical-like surface structure and carbon (Fig. 3b) particles illustrate the nanoplates shaped morphology. The observed particle size from FESEM of α-Fe₂O₃ was around 70–80 nm are higher compared to the average crystallite sizes calculated from XRD analysis and might be ascribed to the larger spherical size because of larger surface area of the smaller crystallites [Jayaraman et al., 2015; Theerthagiri et al., 2013]. The surface morphology of α-Fe₂O₃/C nanocomposite (Fig. 3c) shows that the spherical-like α-Fe₂O₃ nanoparticles are well distributed on the nanoplates-like structure of carbon materials. Moreover, the exhibited surface features of the nanomaterials such as nanoplates and spherical particles can assume a significant role in influencing the cytotoxicity performance.

The composition analysis of α-Fe₂O₃, carbon nanoplates and α-Fe₂O₃/C nanocomposites was determined by EDS and the attained outcomes are depicted in Fig. 4. The EDS spectrum evidently
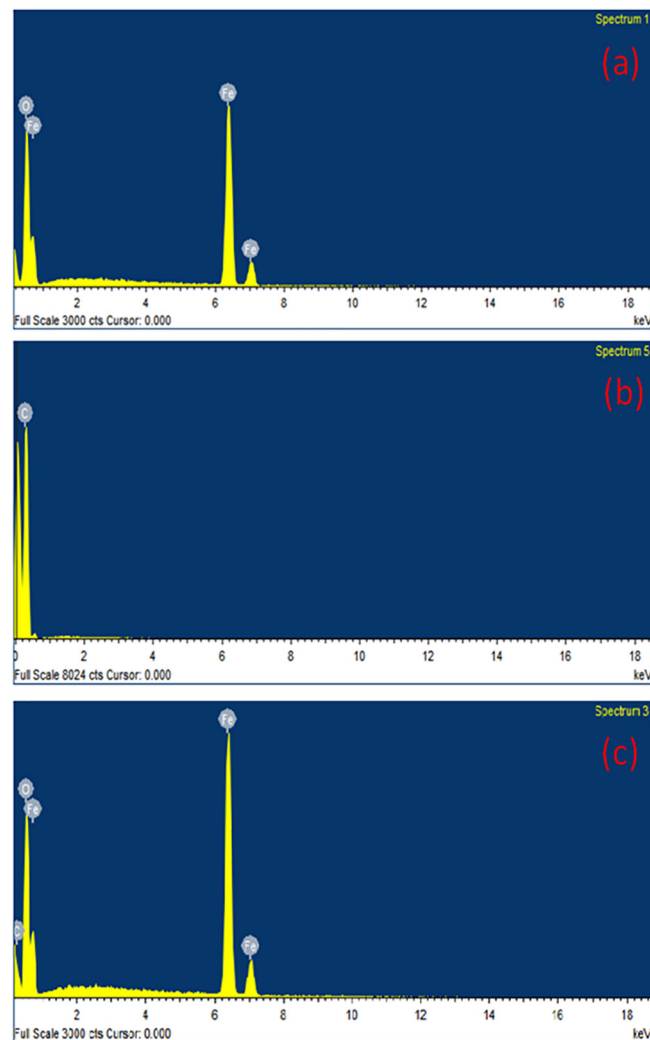

Fig. 2. XRD of (a) α-Fe₂O₃, (b) carbon nanoplates and (c) α-Fe₂O₃/C nanocomposites.

Fig. 3. FESEM images of (a). α-Fe$_2$O$_3$, (b). carbon nanoplates and (c). α-Fe$_2$O$_3$/C nanocomposites.

Fig. 4. EDS spectrum of (a). α-Fe$_2$O$_3$, (b). carbon nanoplates and (c). α-Fe$_2$O$_3$/C nanocomposites.

proved that the pure α-Fe$_2$O$_3$ (Fig. 4a) was composed of Fe and O atoms, and carbon nanoplates (Fig. 4b) consisted of C atoms only without any other impurities. Further, the EDS data of carbon nanoplates incorporated α-Fe$_2$O$_3$ (Fig. 4c) confirmed the existence of corresponding to Fe, O and C atoms. This observation of EDS analysis supports the formation of α-Fe$_2$O$_3$/C nanocomposites.

3.3. MTT assay

The results show that all three samples affected the viability of A549 cells and non cancerous chang liver cells. After 24 h of treatment the viability of cells decreased as the concentration increases. But the cytotoxicity is minimal, the percentage viability is above 70% indicates the nanoparticle doesn't have cytotoxic effects towards normal cells (Fig. 5). Similarly, 50% of inhibition of cells was distinguished in human cancer cell line A549 on optimum concentration (Fig. 6). Among α-Fe$_2$O$_3$, carbon nanoplates and α-Fe$_2$O$_3$/C nanocomposites, higher viability values were observed in α-Fe$_2$O$_3$/C nanocomposites which indicates composite of α-Fe$_2$O$_3$ and carbon has more viability. α-Fe$_2$O$_3$/C nanocomposites showed maximum cell count of 1.5X10^4 cells/well equal to control cells 1.7X10^4 cells/well at 30 μg/mL. The pure nanoparticle showed low cell count such as α-Fe$_2$O$_3$ has 1.17 X10^4 cells/well and carbon has 1.12X10^4 cells/well. The nanoparticles size and surface charge also a main factor for cytotoxicity. Reduction in size of the particles increases bioavailability due to enhanced adsorption. If the particle size is too small it can be cleared through the kidneys, if it is too large trapped by cells. Nanoparticle below 100 nm can able to interact with live cells (10–100 μm) easily than bulk material
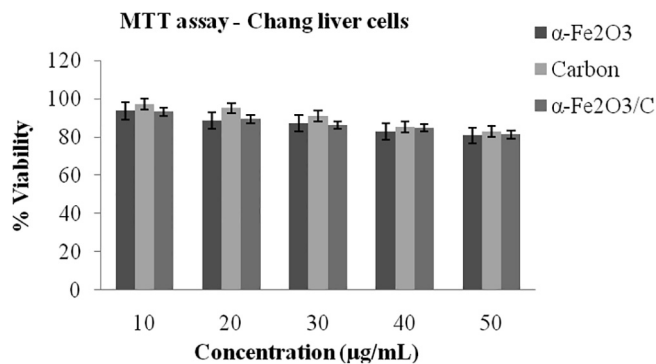
Fig. 5. MTT assay of α-Fe$_2$O$_3$, carbon nanoplates and α-Fe$_2$O$_3$/C nanocomposites non-cancerous cell line (chang liver cells).

[Valdiglesias et al., 2015; Arokiyaraj et al., 2015; Gurusamy et al., 2019; Valsalam et al., 2019]. Konczol et al. (2011) reported that, after 24 h exposure of A549 cells to iron oxide nanoparticle increased mitochondrial membrane depolarization and ROS production. Oxidation-reduction reaction of iron plays main role in DNA synthesis, oxygen transport, mitochondrial oxidative
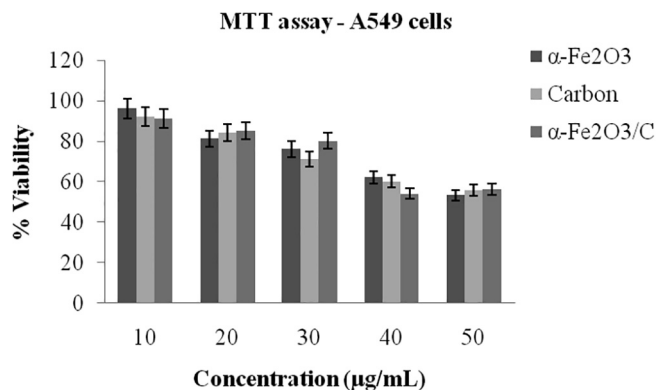
Fig. 6. MTT assay of α-Fe$_2$O$_3$, carbon nanoplates and α-Fe$_2$O$_3$/C nanocomposites non-cancerous cell line (A549 cells).

phosphorylation, and cytochrome P450 function Shander et al., 2009. The obtained cytotoxic activity of α-Fe$_2$O$_3$, carbon nanoplates and α-Fe$_2$O$_3$/C nanocomposites is presented in Table 1.

3.4. Influence of nanomaterial on morphology of cell lines by PI and DAPI staining

Control cells were shown normal morphology and cells were spread in the whole field of microscope. The cell bodies of normal chang liver cells showed normal cell nucleus of cells stayed in the canter and formed a relatively dark area, where as control human lung cancerous cell line showed normal cancerous cell appearance. Nanomaterial administrated for 24 h cells showed changes in to epithelial like, cell shrinkage and condensed cytoplasm, these changes were recorded documented and it is indicated the cells undergoing apoptosis. The activation of apoptosis/cell death is the condition were indicates the cytotoxic effect of the material. The cytotoxic effect of the nanomaterial on cancerous cell lines showed severe effect than the normal non cancerous cell line. Morphology results supports the cytotoxic activity assay based on cell viability after treatment with α-Fe$_2$O$_3$, carbon nanoplates and α-Fe$_2$O$_3$/C nanocomposites Rodrigues et al., 2012 (see Fig. 7).

Cell death induced by α-Fe$_2$O$_3$, carbon nanoplates and α-Fe$_2$O$_3$/C nanocomposites was further confirmed with DAPI. DAPI is the fluorescent dye that stains DNA of live cells. After 48 h of treatment to 30 μg/mL of sample, the cells showed positive to DAPI stain indicates the cells are alive. The effect of α-Fe$_2$O$_3$, carbon and α-Fe$_2$O$_3$/C nanocomposites on cell morphology was depicted in Fig. 6. The fluorescence microscopic images showed more cell number on α-Fe$_2$O$_3$/C nanocomposites treated cells than other nanoparticle but morphology of the nucleus showed no difference when compared to control cells. The images showed the cells have good biocompatibility towards nanoparticle (see Fig. 8).
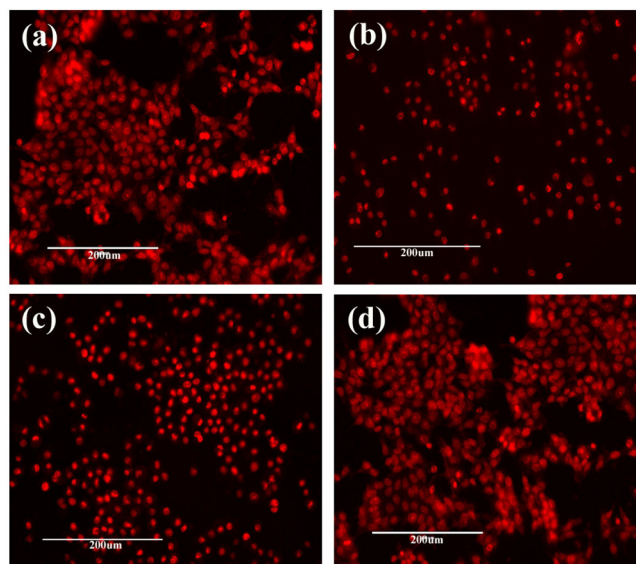

Fig. 7. (a) PI staining of control cells, (b) cells treated with α-Fe$_2$O$_3$/C, (c) α-Fe$_2$O$_3$ and (d) carbon at 30 μg/mL.
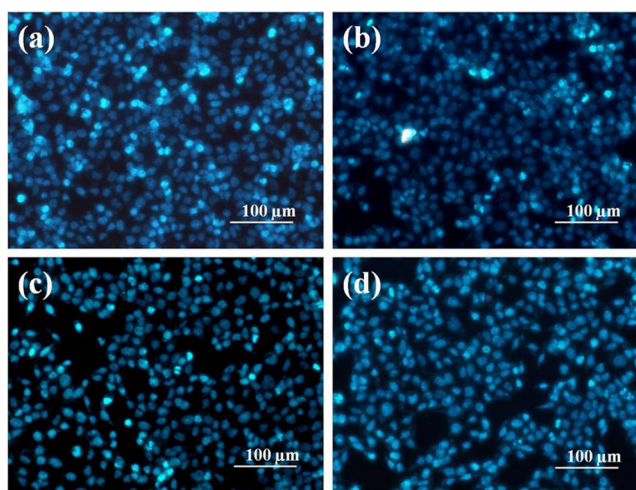

Fig. 8. (a) DAPI staining of control cells, (b) cells treated with α-Fe$_2$O$_3$/C, (c) α-Fe$_2$O$_3$ and (d) carbon at 30 μg/mL.

4. Conclusions

In conclusion, spherical-like α-Fe$_2$O$_3$ was prepared by a low temperature solution combustion route and a α-Fe$_2$O$_3$/C nanocomposite was developed by adding carbon nanoplates on α-Fe$_2$O$_3$ nanoparticles by a wet chemical process. The phase formation of

Table 1
Cytotoxic activity of α-Fe$_2$O$_3$, carbon nanoplates and α-Fe$_2$O$_3$/C nanocomposites on non-cancerous cell line (chang liver cells).

Material	Concentration (μg/mL)				
	10	20	30	40	50
Normal Cells					
α-Fe$_2$O$_3$	93.63	88.74	87.11	83.01	80.94
Carbon	97.29	95.07	91.02	85.24	83.05
α-Fe$_2$O$_3$/C	93.27	89.45	86.32	84.91	81.24
A549 Cells					
α-Fe$_2$O$_3$	96.12	81.26	76.11	62.11	53.29
Carbon	92.12	84.16	71.22	60.22	55.82
α-Fe$_2$O$_3$/C	91.23	85.12	80.23	54.12	56.25

the nanomaterials was examined by XRD analysis. The surface structure and composition of element were revealed by FESEM and EDS analyses. The high toxicity of the material adopted as non-biocompatible for the application in the field of biomedical, drug discovery and therapy. Biocompatibility is normally explained as absence of toxicity, but these are different statements referring to different contexts. Becker et al, defined biocompatibility is the capability of a prosthesis implemented in the body to exist in harmony with tissue without causing deleterious changes. The biocompatibility of the synthesised nano meterials were asssesed by MTT assay and nuclear imaging on non-cancerous chang liver cell and A549 human lung carcinoma cell line. The results demonstrated that the pure and composite material exhibited above 70% viability indicates the α-Fe$_2$O$_3$/C nanocomposite is biocompatible. Thus, the α-Fe$_2$O$_3$/C nanocomposite can be used for different biological applications such as imaging, drug delivery, biosensor, etc. Surface modification must be considered to improve the biocompatibility for implement in biomedical applications.

Acknowledgement

References

Wilkinson, J.M., 2003. Nanotechnology applications in medicine. Med Device Technol 14 (5), 29–31.

Bhattacharya, K., Gogoi, B., Buragohain, A.K., Deb, P., 2014. Fe$_2$O$_3$/C nanocomposites having distinctive antioxidant activity and hemolysis prevention efficiency. Mater. Sci. Eng., C 42, 595–600.

Andiappan, K., Sanmugam, A., Deivanayagam, E., Karuppasamy, K., Kim, H.S., Vikraman, D., 2019. Schiff base rare earth metal complexes: Studies on functional, optical and thermal properties and assessment of antibacterial activity. Int. J. Biol. Macromol. 124, 403–410.

Andiappan, K., Sanmugam, A., Deivanayagam, E., Karuppasamy, K., Kim, H.S., Vikraman, D., 2018. In vitro cytotoxicity activity of novel Schiff base ligand–lanthanide complexes. Sci. Rep. 8, 3054. https://doi.org/10.1038/s41598-018-21366-1.

Wei, Q., Song, P., Yang, Z., Wang, Q., 2018. Hierarchical assembly of Fe$_2$O$_3$ nanorods on SnO$_2$ nanospheres with enhanced ethanol sensing properties. Physica E 103, 156–163.

Sanmugam, A., Vikraman, D., Karuppasamy, K., Lee, J.Y., Kim, Hyun-Seok, 2017. Evaluation of the corrosion resistance properties of electroplated chitosan-Zn1−xCuxO composite. Thin Films Nanomaterials 7 (432). https://doi.org/10.3390/nano7120432.

Theerthagiri, J., Dalavi, Shankar B., Manivel Raja, M., Panda, R.N., 2013. Magnetic properties of nanocrystalline ε-Fe$_3$N and Co$_4$N phases synthesized by newer precursor route. Mater. Res. Bull. 48, 4444–4448.

Patsula, V., Moskvin, M., Dutz, S., Horák, D., 2016. Size-dependent magnetic properties of iron oxide nanoparticles. J. Phys. Chem. Solids 88, 24–30.

Rajendran, K., Sena, S., Suja, G., Senthil, S.L., Vinoth Kumar, T., 2017. Evaluation of cytotoxicity of hematite nanoparticles in bacteria and human cell lines. Coll. Surf. B Biointerf. 157, 101–109.

Cardillo, D., Tehei, M., Hossain, Md.S., Islam, Md.M., Bogusz, K., Shi, D., Mitchell, D., Lerch, M., Rosenfeld, A., Corde, S., Konstantinov, K., 2016. Synthesis-dependent surface defects and morphology of hematite nanoparticles and their effect on cytotoxicity in vitro. ACS Appl. Mater. Interf. 8 (9), 5867–5876.

Kanagesan, S., Hashim, M., Tamilselvan, S., Alitheen, N.B., Ismail, I., Hajalilou, A., Ahsanul, K., 2013. Synthesis, characterization, and cytotoxicity of iron oxide nanoparticles. Adv. Mater. Sci. Eng. 2013, 1–7. https://doi.org/10.1155/2013/710432.

Rajendran, K., Karunagaran, V., Mahanty, B., Sen, S., 2015. Biosynthesis of hematite nanoparticles and its cytotoxic effect on HepG2 cancer cells. Int. J. Biol. Macromol. 74, 376–381.

Theerthagiri, J., Senthil, R.A., Priya, A., Madhavan, J., Michael, R.J.V., Ashokkumar, M., 2014. Photocatalytic and photoelectrochemical studies of Visible-light active α-Fe$_2$O$_3$-g-C$_3$N$_4$ nanocomposites. RSC Adv. 4, 38222–38229.

Senthil, R.A., Priya, A., Theerthagiri, J., Selvi, A., Nithyadharseni, P., Madhavan, J., 2018. Facile synthesis of α-Fe$_2$O$_3$/WO$_3$ composite with an enhanced photocatalytic and photo-electrochemical performance. Ionics. https://doi.org/10.1007/s11581-018-2473-y.

Rajan, A.S., Sampath, S., Shukla, A.K., 2014. An in situ carbon-grafted alkaline iron electrode for iron-based accumulators. Energy Environ. Sci. 7, 1110–1116.

Theerthagiri, J., Senthil, R.A., Buraidah, M.H., Madhavan, J., Arof, A.K., Ashokkumar, M., 2016. One-step electrochemical deposition of Ni$_{1-x}$Mo$_x$S ternary sulfides as an efficient counter electrode for dye-sensitized solar cells. J. Mater. Chem. A 4, 16119–16127.

Jayaraman, T., Raja, S.A., Priya, A., Jagannathan, M., Ashokkumar, M., 2015. Synthesis of a visible-light active V$_2$O$_5$–g-C$_3$N$_4$ heterojunction as an efficient photocatalytic and photoelectrochemical material. New J. Chem. 39, 1367–1374.

Valdiglesias, V., Kiliç, G., Costa, C., Fernández-Bertólez, N., Pásaro, E., Teixeira, J.P., Laffon, B., 2015. Effects of iron oxide nanoparticles: cytotoxicity, genotoxicity, developmental toxicity, and neurotoxicity. Environ. Mol. Mutagen. 56 (2), 125–148.

Konczol, M., Ebeling, S., Goldenberg, E., Treude, F., Gminski, R., Giere, R., Grobety, B., Rothen-Rutishauser, B., Merfort, I., Mersch-Sundermann, V., 2011. Cytotoxicity and genotoxicity of size-fractionated iron oxide (magnetite) in A549 human lung epithelial cells: role of ROS, JNK, and NF-κB. Chem. Res. Toxicol. 24 (9), 1460–1475.

Shander, A., Cappellini, M.D., Goodnough, L.T., 2009. Iron overload and toxicity: The hidden risk of multiple blood transfusions. Vox Sang 97, 185–197.

Rodrigues, S., Dionísio, M., López, C.R., Grenha, A., 2012. Biocompatibility of chitosan carriers with application in drug delivery. J Funct. Biomater. 3 (3), 615–641.

Basith, N.M., Raj, R.A., AlSalhi, M.S., Devanesan, S., Askar Ali, S.J., Rajasekar, S., Sundaram, R., Ragupathi, C., 2016. 2016 Structural, magnetic, optical, and catalytic properties of Fe$_3$O$_4$ nanoparticles by the sol-gel method. J. Supercond. Novel Magnet 29 (8), 2053–2058.

AlSalhi, M.S., Devanesan, S., Alfuraydi, A.A., Vishnubalaji, R., Munusamy, M.A., Murugan, K., Nicoletti, M., Benelli, G., 2016. 2016 Green synthesis of silver nanoparticles using Pimpinella anisum seeds: antimicrobial activity and cytotoxicity on human neonatal skin stromal cells and colon cancer cells. Int. J. Nanomed. 11, 4439.

Valsalam, S., Agastian, P., Esmail, G.A., Ghilan, A.K.M., Al-Dhabi, N.A., Arasu, M.V., 2019. Biosynthesis of silver and gold nanoparticles using Musa acuminata colla flower and its pharmaceutical activity against bacteria and anticancer efficacy. J. Photochem. Photobiol. B. https://doi.org/10.1016/j.jphotobiol.2019.111670.

Gurusamy, S., Kulanthaisamy, M.R., Hari, D.G., Veleeswaran, A., Thulasinathan, B., Muthuramalingam, J.B., Balasubramani, R., Chang, S.W., Arasu, M.V., Al-Dhabi, N.A., Selvaraj, A., Alagarsamy, A., 2019. Environmental friendly synthesis of TiO2-ZnO nanocomposite catalyst and silver nanomaterials for the enhanced production of biodiesel from Ulva lactuca seaweed and potential antimicrobial properties against the microbial pathogens. J. Photochem. Photobiol. B 193, 118–130.

Arokiyaraj, S., Saravanan, M., Badathala, V., 2015. Green synthesis of Silver nanoparticles using aqueous extract of Taraxacum officinale and its antimicrobial activity. South Indian J. Bioogical Sci. 2, 115–118.